Surface Science 606 (2012) 1393–1399

Contents lists available at SciVerse ScienceDirect

Surface Science

journal homepage: www.elsevier.com/locate/susc

The effect of substrate roughness on the static friction of CuO nanowires

Boris Polyakov [a,c,*], Sergei Vlassov [a], Leonid M. Dorogin [a], Peteris Kulis [c], Ilmar Kink [a,b], Rynno Lohmus [a]

[a] Institute of Physics, University of Tartu, Riia st. 142, 51014, Tartu, Estonia
[b] Estonian Nanotechnology Competence Centre, Riia 142, 51014, Tartu, Estonia
[c] Institute of Solid State Physics, University of Latvia, Kengaraga st. 8, LV-1063, Riga, Latvia

ARTICLE INFO

Article history:
Received 1 February 2012
Accepted 28 April 2012
Available online 8 May 2012

Keywords:
Nanotribology
Nanomanipulation
In situ electron microscopy
Copper oxide nanowires
Surface roughness
Adhesion
Static friction

ABSTRACT

The dependence of static friction on surface roughness was measured for copper oxide nanowires on silicon wafers coated with amorphous silicon. The surface roughness of the substrate was varied to different extent by the chemical etching of the substrates. For friction measurements, the nanowires (NWs) were pushed by an atomic-force microscope (AFM) tip at one end of the NW until complete displacement of the NW was achieved. The elastic bending profile of a NW during this manipulation process was used to calculate the ultimate static friction force. A strong dependence of static friction on surface roughness was demonstrated. The real contact area and interfacial shear strength were estimated using a multiple elastic asperity model, which is based on the Derjaguin–Muller–Toporov (DMT) contact mechanics. The model included vertical elastic flexure of NW rested on high asperities due to van der Waals force.

© 2012 Elsevier B.V. All rights reserved.

1. Introduction

It is well known that the laws of friction at the nanoscale differ significantly from their macroscale counterparts and that one of the most relevant issues in nanotribology is the dependence of friction on the real contact area. Tribology of nanoscale contacts has been intensively investigated using AFM microscopy methods [1,2]. However, the contact area in this case could not be easily scaled up due to the small and well-defined radii of commercial AFM tips. Hence, the manipulation of metal clusters of different sizes and arbitrary shapes by AFM tips have been used as scalable objects for studying friction in contacts of intermediate sizes [3]. It should be noted that the actual contact area between the substrate surface and arbitrarily shaped nanoparticles is not well defined. Hence, NWs with their well-defined shapes are the near-perfect candidates to bridge the gap between the nano and microscale friction.

The mechanical and electrical properties of single-crystal nanowires can be superior in comparison to corresponding bulk material [4]. For instance, semiconductor NWs have demonstrated remarkable optical, electronic, magnetic, piezoelectric and piezoresistive characteristics [4–6]. NWs and nanotubes (NT) have potential applications in electronic, opto-electronic nanodevices and sensors, as well as in microelectromechanical systems (MEMS) and nanoelectromechanical systems (NEMS) [7–11].

MEMS and NEMS have a wide spectrum of applications, from traditional resonance-frequency devices, accelerometers and pressure sensors to novel devices, such as micromanipulators, piezoelectric gated diodes and nanorelays [9,12]. In scaling down the dimensions of MEMS devices, one has to consider that surface forces (adhesion and friction) began to play an increasingly important role in device performance and reliability, due to the large surface-to-volume ratio of MEMS and NEMS. Moreover, friction and adhesion, which lead to wear and stiction, are common causes of failure in MEMS. Hence, a detailed understanding of adhesion and friction phenomena at the nanoscale is essential for the successful engineering of high performance MEMS and NEMS devices.

Currently, the phenomena of adhesion and static friction for NWs and NTs are poorly explored. Only a few works have been dedicated to the study of NW- or NT-substrate adhesion and friction. For instance, Bordag et al. proposed a method for measuring the distributed static friction of NWs on flat substrates [13]. They used the radius of curvature of the maximum NW bending after manipulation and Young's modulus of the corresponding material as inputs for the calculation of static friction. This method was further developed by Strus et al. for carbon NTs [14] and Dorogin et al. for ZnO NWs [15].

Manoharan et al. investigated adhesion and kinetic friction of long ZnO NWs on smooth silicon wafers [16]. They showed that the friction coefficient for the ZnO nanowires and silicon wafer system can be approximately two orders of magnitude higher than their corresponding bulk values at ambient conditions. On smooth surfaces, when the actual contact area is comparable to the apparent contact area, static friction forces can be extremely high, and the interfacial shear stress can exceed the ultimate strength of the NW,

* Corresponding author at: Institute of Physics, University of Tartu, Riia st. 142, 51014, Tartu, Estonia.
E-mail address: boriss.polakovs@ut.ee (B. Polyakov).

0039-6028/$ – see front matter © 2012 Elsevier B.V. All rights reserved.
doi:10.1016/j.susc.2012.04.029

which can result in NW rupture during manipulation. For example, rupture was reported by Hsu et al. for BN NWs manipulated on a silicon wafer surface [17].

The time dependence of static friction or contact aging is another important challenge in nanotribology. For instance, this phenomenon was observed in gold nanoparticles at ambient conditions [18] and in vacuum [19]. However, a comprehensive explanation of contact aging is still lacking. This contact-aging phenomenon may be closely related to the large difference between static and kinetic friction found for the nanowires and nanoparticles [19,20].

It is known that macroscopic friction is proportional to normal load. In nanoscale objects, gravitational force is negligibly small, and if no external load is applied, then van-der-Waals (vdW) attractive forces between contacting surfaces act as the effective normal loading force that determines the friction [21]. VdW forces can be significantly reduced using precisely controlled nanometer-scale surface roughness or specially patterned surfaces. For typical surfaces, macroscopic friction is usually nearly independent of the surface roughness, unless the surfaces are either very rough or very smooth [21]. However, in nanoscopic systems, roughness of the contacting surfaces is directly associated to the actual contact area and the average distance between them. The effect of nanoscale roughness on adhesion for MEMS has been addressed in many works [22,23]. However, in most nanomanipulation experiments performed on NWs the apparent (instead of real) contact area of the NW and substrate was used in the calculation of interfacial shear stress [13,16,17].

In this article, we investigated the effect of surface roughness on the NW-substrate static friction. We made an attempt to calculate the interfacial shear strength for static friction using real contact area in the framework of the DMT model. Real contact area and vdW attraction force between the NW and substrate surface was calculated for different substrate roughness using actual AFM images of the surfaces, and then correlated with the measured static friction force. To the best of our knowledge, no prior work has been performed on NW static friction dependence on substrate roughness.

2. Theory

In our previous work we presented a method that enables estimation of the NW-substrate maximal static friction force from NW nanomanipulation experiments, NW is pushed at one end by an AFM tip, while the opposite end of the NW remained adhered to the substrate (Fig. 1). When the elastic stress generated inside the bent NW overcomes the total static friction force, the entire NW is displaced. The bending profile of the NW just before its complete displacement ("most bent state") is then used to calculate the ultimate static friction (and corresponding interfacial shear strength). This method implies that the Young's modulus of the NW is known, in addition to other details of the system as described in [24].

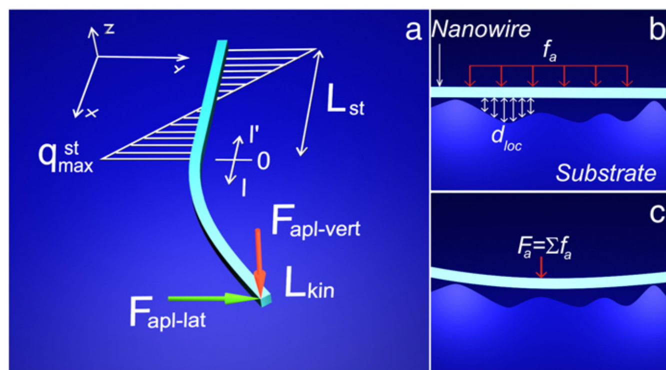

Fig. 1. Schematic of a NW on substrate static friction measurement. (a). NW rests on high asperities, before vertical deflection; (b). NW bends vertically due to vdW attraction force, decreasing average NW-substrate distance (c). Substrate roughness and vertical deflection of NW are exaggerated for better visibility.

In this work we used the value of Young's modulus taken from the work of Tan et al. [25]. They measured Young's modulus of CuO NWs by performing a three-point bend test with an AFM. The Young's modulus of the NWs was in the range of 70 to 300 GPa. We chose the minimal value of 70 GPa to ensure conservative estimates of the static friction in our calculations.

The "most bent state" is sustained in equilibrium due to the interplay of intrinsic elastic force in the NW, the lateral forces of friction from the substrate, and the driving force of the AFM tip. The full system of equations for the equilibrium of the NW comprises the equations for elastic force F and for the momentum M in the cross-section of the NW [26]. The reduced equilibrium equation for the profile of bent part of the NW can be written in terms of the tangent angle φ as a function over the NW length l over the interval $[0, L_{kin}]$, assuming that the NW is purely bent:

$$EI\frac{d^2\phi}{dl^2} = \left[q^{kin}(l-L_{kin})-F_{apl-lat}\right]\cdot\cos(\varphi+\theta)$$
$$\phi\Big|_{l=o} = o \qquad (1a, b, c)$$
$$\frac{d\phi}{dl}\Big|_{l=L_{kin}} = 0$$

where E is the Young's modulus of the NW, I is the area moment of inertia of the cross section, and θ is the angle between the vector of applied external force and the y axis.

The kinetic friction force can be considered to be small compared to the static friction force and can therefore be neglected [24]. Thus, the internal elastic force is constant over the interval $[0, L_{kin}]$ and equal to the applied external force $F=F_{apl\text{-}lat}$. The momentum of elastic forces as a function along the NW axis can be written as $M=EI\frac{d\varphi}{dl}$.

The motionless ("static") part of the NW is assumed to be a rigid rod of length L_{st}. The values of the elastic force $F|_{l=0}$ and momentum $M|_{l=0}$ at the starting point of the motionless region follow from the solution of Eq. (1a,b,c) based on the condition for continuity. For simplicity, we assume that the interfacial shear stress between the NW and the substrate and, consequently, the static friction force, are distributed linearly along the rotated static part of the NW: $q^{st}_y(l')=a\cdot l'+b$, where a and b are unknown constants. To maintain equilibrium of the NW, the conditions for total force and momentum yield a system of two equations:

$$F\Big|l=0 = \int_0^{L_{st}} q^{st}_y\left(l'\right)dl' \qquad (2a, b)$$

$$M\Big|l=0 = \int_0^{L_{st}} q^{st}_y\left(l'\right)l'dl',$$

which can be easily used to determine a and b. Then, parameters such as the maximum static friction:

$$q^{st}_{\max} = |b|, \qquad (3a)$$

and averaged static friction can be determined (Fig. 1a):

$$q^{st}_{avg} = \int_0^{Lst}\left|q^{st}_y(l)\right|dl. \qquad (3b)$$

3. Material and methods

To prepare substrates with different roughness values, amorphous silicon (a-Si) was first deposited on thermally oxidized silicon wafers (*Alfa RPAR*) by e-beam evaporation followed by etching with a

"Secco" solution (K_2CrO_3: HF: H_2O) to different degrees. The unetched substrate had minimal surface roughness (substrate Nr.1, "*smooth*"). "*Small roughness*" was obtained by etching in a water-diluted "Secco" solution (1:5) for a total etching time of 15 s (substrate Nr.2). A concentrated "Secco" solution was used to prepare a "*high roughness*" substrate using an etching time of 1 s (substrate Nr.4). The region bordering the etched and non-etched areas was used as a "*Medium roughness*" surface (substrate Nr.3). An AFM (*Veeco*, Dimension Edge, *Olympus* cantilevers) was used to measure the resulting surface roughness in tapping mode at ambient conditions.

CuO NWs were grown by heating copper foil at 400 °C in an open-ended quartz tube over a period of 2 h [27]. Synthesized NWs were 10–20 μm long and had diameters in the range of 50 to 150 nm. The X-ray diffraction (XRD) pattern was recorded from as-prepared oxidized copper foil sample covered with NWs using a X'Pert Pro MPD diffractometer (*PANalytical*) in 2θ ranging from 10 to 80° using Cu Kα radiation (λ = 1.5406 Å). Analysis of XRD patterns reveals presence of Cu_2O, Cu and CuO phases similar to [27,28]. Peaks at 35.55, 38.80° correspond to (11–1) and (111) planes of monoclinic CuO, peaks at 29.60, 36.47, 42.30, 61.36° to (110), (111), (200), (220) planes of cubic Cu_2O, peaks at 43.35, 50.49 and 74.19° to (111), (200) and (220) planes of cubic Cu. As it was shown in [27] growth direction of CuO NWs are [111] and [11-1] directions which agrees with our results.

After growth, the NWs were transferred to substrates with different roughness. A large fraction of the NWs was broken into shorter pieces (several microns long) during the transfer process. Energy-dispersive X-ray (EDX) spectra were recorded by Helios NanoLab 600 electron-ion dual beam microscope equipped with an EDS detector (50 mm² X-Max SDD detector, *Oxford Instruments*). The spectra were analyzed using standard procedures provided by INCA software (*Oxford Instruments*). The estimated accuracy of quantitative results of the element analysis is better that 2%. EDX signal measured on CuO NW shows nearly equal amount of copper (0.95 keV) and oxygen (0.5 keV), and presence of silicon (1.75 keV) (due to semi-transparency of NW). Signal measured on etched a-Si substrate shows silicon line and some amount of oxygen, probably due to formation of natural oxide layer on silicon.

NW-manipulation experiments were performed inside a scanning electron microscope (*TESCAN Vega-II SBU*) in vacuum at 3×10^{-4} mbar at room temperature. Contact mode AFM cantilevers (*Nanosensor* AdvancedTEC-CONT cantilevers; force constant 0.2 N/m; nominal tip radius, 10 nm) were used for NW manipulation. The geometry of the cantilevers enabled tip visibility from the top view. The AFM chip was mounted on a three-dimensional nanomanipulator equipped with position sensors (SLC-1720-S, *SmarAct*) and installed inside the SEM.

For manipulation of NWs, the AFM chip was brought into contact with the substrate surface and then lowered further by 5–15 μm (1–3 μN) to ensure that the applied force was sufficient to displace NWs in the lateral direction. Although AFM cantilevers were used as probes, no AFM feedback loop was used in the experiment. Nonetheless, a near-constant loading force was ensured during manipulation by moving the nanomanipulator along the direction that was parallel to the surface.

4. Results

We observed four different scenarios of NW behavior during manipulation. At high static friction forces, NWs either could not be displaced at all or broke into shorter pieces without bending (Fig. 2a–d). At smaller static friction forces, NWs were gradually displaced from one end of the NW, with the other end fixed by the static friction force. If the static friction force exceeded the ultimate strength of the NW, the NW would break (Fig. 2e–h). If static friction force was smaller than the NW interfacial shear strength, the NW was displaced as an entire object (Fig. 2i–l). Only in this scenario the "most bent state" of the NW could be found (Fig. 2k). For very small static friction forces in comparison with the NW elastic force ("zero static friction") the NW was displaced as a rigid rod without noticeable bending (Fig. 2m–p). Taking into account such distinctive behavior, we qualitatively compared the NW static friction on substrates with different roughness considering the frequency of occurrence for each scenario.

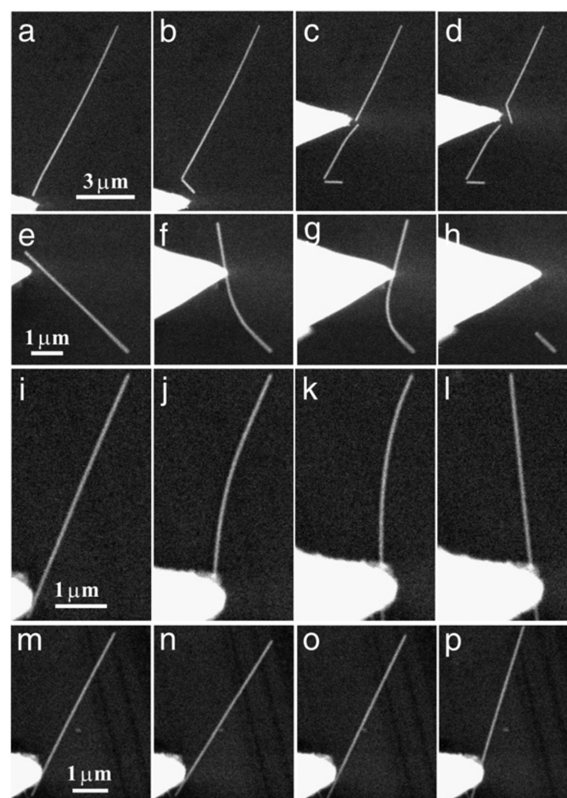

Fig. 2. Four different scenarios of NW behavior during manipulation. Crashed or motionless: the NW was broken into pieces during manipulation (a–d). Bent and broken: the NW was displaced partially and then broken (e–h). Bent and displaced: the NW was successfully displaced (i–l). The "most bent state" of the NW before complete displacement can be observed at frame (k). "Zero static friction": the NW was displaced as a rigid rod and static friction was too small to cause NW bending (m–p).

NW manipulation statistics on substrates of different roughness are summarized in Table 1. Cross sections of the AFM topography for each surface are shown in Fig. 3a. The root mean squared roughness (R_{RMS}) for all substrates used in our experiment as characterized by AFM are given in Table 2. It is evident that the higher the surface roughness, the easier it is to move the NWs. On the contrary, the smaller the roughness of surfaces, the "closer" the two surfaces can be and hence, the higher the vdW force, and consequently, the higher the adhesion and static friction.

Table 1
Statistics of NW behavior during manipulation on substrates of different roughness.

Substrate nr.	"Zero" friction NWs	Bent and displaced NWs	Bent and broken NWs	Crashed or motionless NWs	Total, NWs
1. Smooth (unetched)	0	5 (11%)	19 (40%)	24 (50%)	48
2. Small roughness	0	13 (33%)	12 (31%)	14 (36%)	39
3. Medium roughness	0	26 (54%)	17 (35%)	5 (11%)	48
4. High roughness	10 (24%)	26 (62%)	6 (14%)	0	42

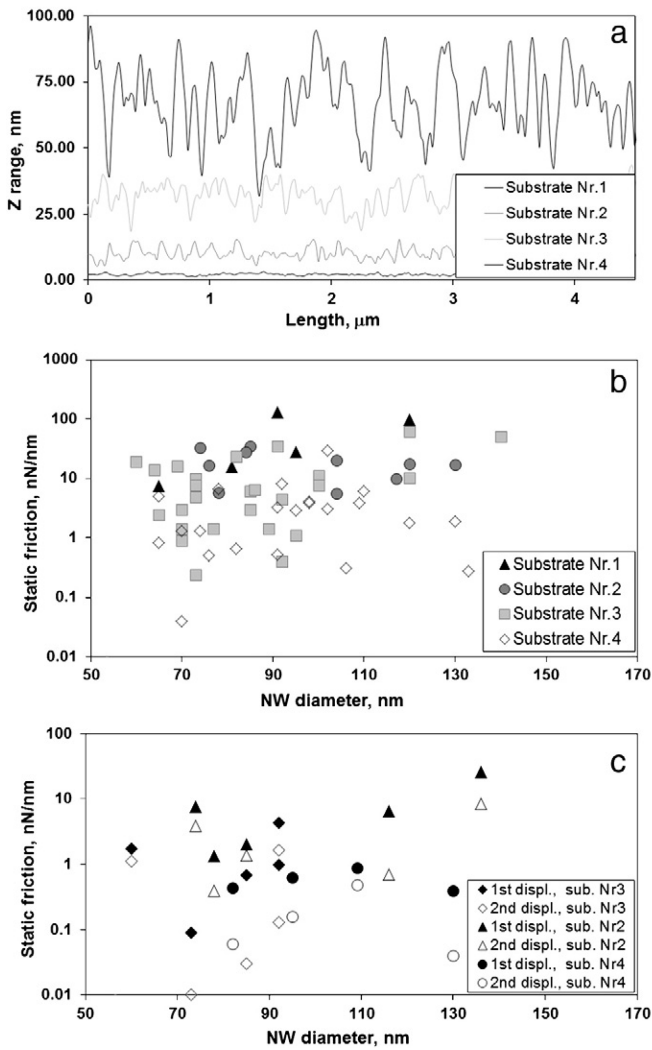

Fig. 3. AFM line topography of the substrates of different roughness (a). Averaged static friction of NWs on substrates of different roughness measured by the bending profile method via the nanomanipulation experiments (b). Static friction for the first and second displacement of the NW measured via the nanomanipulation experiments (c).

Numerical values of static friction forces were calculated for the cases when the NW was bent and displaced using its "most bent state" profile (third scenario, Fig. 2k). Data on averaged static friction q^{st}_{avg} for all substrates is summarized in Table 2. A significant decrease in static friction with increasing surface roughness is evident. However, it is necessary to note that this statistic does not take into account the case of "zero static friction" (friction below the sensitivity of the method) and crashed/motionless NWs (friction beyond the sensitivity of the method). Hence, the averaged static friction might be underestimated for substrate Nr.1 ("*smooth*") and Nr.2 ("small roughness"), but overestimated for substrate Nr.4 ("*high roughness*").

It should be noted that a large variation in values of static and kinetic friction is a common phenomenon for NWs. For example, variations of more than an order of magnitude were observed by Conache et al. in the friction measurements of InAs NWs on a Si_3N_4 substrate [20]. In our experiments we can identify three possible sources of uncertainties. First, we used a single value of Young's modulus for all NWs while actual values of Young's moduli of CuO nanowires can vary by a factor of four [25]. Second, deviation of the NW geometry from a rectangular cross-section changes the moment of inertia significantly and might introduce a significant error in the static force calculation. Third, asperities have a random distribution of heights, which might lead to cases when NW relies on asperities much higher than the average height of the surface resulting in low vdW attraction forces and, hence, low static friction. As a result of the aforementioned reason, minimal scattering of static friction values can be observed (Fig. 3b) on substrate Nr.1 ("*smooth*") and large scattering can be observed on substrate Nr. 4 ("*high roughness*"). However, our averaged data is based on measurements made on numerous NWs (70 NWs in total), and therefore can be considered as a reliable valuation of the effect of roughness on static friction.

For some NWs that were in static contact with a substrate for several hours we re-measured the static friction within minutes after the first displacement. We found decrease in static friction in the second and subsequent trials by factor ranging from 1.5 up to 23 times (6 times in average) in comparison to that of the initial displacement. Values of static friction for the first and second displacements are presented in Fig. 3c. This effect can be interpreted as contact aging [18] as discussed in more detail in the Discussion section.

5. Modeling

For better understanding the static friction dependence on substrate roughness, we made an attempt to estimate vdW forces and real contact area between a NW and substrate. We adopted the vdW force calculation method of Delrio et al., where substrate topography data was directly exported from AFM files. Such approach enables avoiding the usage of any statistical models of surface roughness commonly used in contact mechanics (e.g., Majumdar–Bhushan model, Persson model, etc.).

Contact mechanics analysis was performed for a model of 1000 nm long ideal NWs having a square cross section of 100 × 100 nm. Parameters of the NW were chosen based on their SEM images, and the fact that CuO NWs belong to the monoclinic crystal system [29] and have rectangular cross-sections with well-defined facets [30]. Therefore, 100 × 1000 nm stripes corresponding to facets of NWs were chosen over an area of 1000 × 1000 nm in the AFM images as data sources for the calculation of the vdW force F_a. The mathematical plane touching three highest asperities, as the minimal number of supporting points needed to hold NW, was found at condition not intersect other asperities. Three asperities are expected to be the points of initial contact with the flat NW facet.

Table 2
Correlation between experimentally measured static friction and substrate roughness, and calculated van der Waals force (before and after deformation of contacting asperities), contact area with and without vertical deflection of NW, and interfacial shear strength.

Substrate nr.	R_{RMS}, nm	Aver. static friction, nN/nm	Theor. contact area S_{theor}, nm^2	F_a force, before deflection, nN	F'_a force, after deflection, nN	Contact area before deflection S_r, nm^2	Contact area after deflection S'_r, nm^2	Interf. shear stren., GPa
1. Smooth (unetched)	0.7	5.8	4462	571	9975	421	7004	0.8
2. Small roughness	2.1	3.9	3000	274	877	220	647	6.0
3. Medium roughness	5.4	1.4	1077	121	125	87	92	15.2
4. High roughness	16.1	0.6	462	116	116	92	95	6.3

In the next step we calculated the depth of elastic deformation of asperities in direct contact with the NW. Contact area of elastically deformed asperity and deformation depth can be calculated by DMT model of elastic contacts [4,31]:

$$\delta = \frac{a_r^2}{R}, \tag{4a}$$

where

$$a_r = \sqrt[3]{\frac{2\pi W_A R^2}{K}}, \tag{4b}$$

where a_r is radius of contact, δ is the asperity deformation depth, R is the radius of asperity and W_A is the work of adhesion. The average radii of asperities found from AFM images were $R=400$, 90, 75 and 50 nm for the substrates Nr.1, Nr.2, Nr.3 and Nr.4, respectively. K is reduced elastic modulus:

$$K = \frac{4}{3}\cdot\left[\left(1-\nu_1^2\right)/E_1 + \left(1-\nu_2^2\right)/E_2\right]^{-1}, \tag{5}$$

where $E_1=80$ GPa, $E_2=70$ GPa are the Young's moduli, $\nu_1=0.22$ and $\nu_2=0.3$ are Poisson's ratios of a-Si and CuO, respectively [25,32], yielding reduced elastic modulus $K=53$ GPa. Hamaker constant A_{12} for CuO/Si system in vacuum can be calculated as following [35]:

$$A_{12} = \sqrt{A_{CuO}\cdot A_{Si}}. \tag{6}$$

Hamaker constant of silicon is 25.5×10^{-20} J [33]. Hamaker constant for CuO, as calculated from its surface energy 29.34×10^{-3} J/m^2 [34], is $A_{CuO}=6.2\times10^{-20}$ J. The work of adhesion W_A can be estimated as [4]:

$$W_A = \frac{A_{12}}{12\pi d_{co}^2} \approx 0.1217 \quad \mathrm{J/m^2}, \tag{7}$$

where the cutoff distance $d_{co}=0.165$ nm [35].

The attractive vdW force F_a between the NW and substrate was calculated by Delrio et al. method [23,36]:

$$F_a = \frac{S}{N_{pixels}}\left[\sum_{pixels}\frac{A_{12}}{6\pi(d_{loc}-\delta+d_{co})^3}\right], \tag{8}$$

where S is the NW-substrate nominal (apparent) contact area, N_{pixels} is the number of AFM scan pixels in the NW area, d_{loc} represents the local gap between NW and substrate at each individual pixel (taken directly from AFM data file). Attractive vdW forces F_a calculated for ideal 100×1000 nm NW on substrate of different roughness are presented in Table 2.

As it was stated before, an ideal rigid NW rests on three highest asperities. Real contact area S_r was defined as area of substrate surface located closer to NW facet than cutoff distance d_{co} after asperity deformation calculated by DMT model (Table 2). However, NWs can not be considered as absolutely rigid rods. NW can deflect vertically due to attractive vdW force. The smaller is NW diameter, the more pronounced become NW deflection. Vertical deflection results in increase of NW-substrate contact area due to formation of new contacts with underlying asperities.

In order to account for deflection of the NW under vdW forces, we have used a simple model based on the elastic beam theory [26]. Four intervals including the previously found three highest asperities were considered in the longitudinal direction: first free end of NW–1st asperity, 1st asperity–2nd asperity, 2nd asperity–3rd asperity, and 3rd asperity–second free end of NW. Only one interval providing the largest deflection was selected by estimation of the characteristic momentum $M_i=F_{ia}L_i$, where F_{ia} is the total vdW force acting on the interval L_i. Then, two intervals (sections) are considered: section between two asperities, and section between asperity and free end of NW.

In the first case, the model of an elastic beam between two supporting stands with concentrated load in the middle was used (Fig. 1b, c). For the second case, the model of a "clamped" beam loaded at the end was employed. Concentrated load gives approximately two times higher deflection than the load uniformly distributed along the beam. Therefore, for both sections, the load force was computed as a half of the corresponding vdW force on the selected interval. The deflection profile obtained according to the chosen model was then used to recalculate the contact area S'_r and the vdW force F'_a (Table 2). It is important to note, that the described calculations are rough and have a goal only to demonstrate the importance and the order of magnitude of the deflection effect and can differ much from the actual deflection profile. Noteworthy, values in the Table 2 are averaged over 5 stripes (results for all stripes are given in the *Supplementary data* file). Due to random distribution of heights and positions of asperities the deflection effect on surface area can vary few orders of magnitude. This agrees well with large dispersion of experimentally obtained static friction values (Fig. 3b). As it can be seen the effect of vertical deflection of NW on contact area can be significant for substrates with small roughness. But this effect is negligible for high roughness substrates due to large average NW-substrate distance.

6. Discussion

The friction force at the nanoscale is proportional to the real contact area, that is, $F_{\mathrm{friction}}=\tau S_r$, where τ is the interfacial shear stress and S_r is the real contact area [37]. Bhushan and Nosonovsky proposed a hypothesis for the scale dependence of interfacial shear strength, wherein interfacial shear strength has a tendency to increase for nanoscale contacts [38]. Values of interfacial shear strength determined in AFM experiments could be almost two orders of magnitude higher than the ones found in Surface Force Apparatus (SFA) experiments. The upper limit of shear strength is a theoretical value, which can be obtained from the relation $\tau_{theor}=G^*/2\pi$, where G^* is the combined shear modulus [39]. We calculated $\tau_{theor}=1.3$ GPa, using a value of the combined shear stress $G^*=8.5$ GPa. Combined shear modulus can be calculated as follows [39]:

$$G^* = \left[(2-\nu_1)/G_1 + (2-\nu_2)/G_2\right]^{-1}, \tag{9a}$$

$$G = E/2(1+\nu). \tag{9b}$$

It is well known that for macroscopic bodies in contact the real contact area is several orders of magnitude smaller than the apparent contact area [21]. In mesoscopic or nanoscale friction experiments, real contact areas may be comparable with apparent contact areas due to the relatively small summit heights of asperities in the contact region. The real contact area was 7% of the apparent contact area, which was ~10^5 nm^2 (for a NW 100×1000 nm^2) for substrate Nr.1 ("*smooth*"), 0.7% for substrate Nr.2 ("*small roughness*"), 0.1% for substrate Nr.3 ("*medium roughness*") and 0.1% for substrate Nr.4 ("*high roughness*"). However, if we use theoretical interfacial shear strength $\tau_{theor}=1.3$ GPa and calculate real contact area from static friction values, it will result in contact areas 4.5% (4462 nm^2), 3% (3000 nm^2), 1.1% (1077 nm^2) and 0.5% (462 nm^2) for substrates Nr.1, Nr.2, Nr.3 and Nr.4 respectively (Table 2). We estimated interfacial shear strength dividing the experimentally measured averaged static friction by calculated contact area S'_r. We found $\tau_{exp}=0.8$ GPa for substrate Nr.1, 6.0 GPa for Nr.2, 15.2 GPa for Nr.3 and 6.3 GPa for Nr.4. Calculated values of τ_{exp} are higher than τ_{theor}, obviously indicating underestimated real contact area. Note, that values of averaged static friction q_{avg} used for τ_{exp} calculations were taken for the first displacement of NWs (Fig. 3c).

As was already mentioned above, during the second displacement of NW static friction was about 6 times smaller than for the first one, resulting in 6 times smaller interfacial shear strength (τ_{exp} equal to 1.0, 2.5, 1.1 GPa for substrates Nr.2, Nr.3 and Nr.4 respectively).

In most previous works on NW-substrate friction, interfacial shear strength was normalized by the apparent contact area and, thus, cannot be directly compared to our τ_{exp} data. Only the results of experiments that reported the real contact area can be used for comparison. For example, Carpick et al. performed friction studies by AFM on mica and platinum tips in vacuum and found values of interfacial shear strength of 0.9 GPa [40], which is comparable with calculated values of τ_{exp} value in our experiments.

We suppose that significant difference between interfacial shear strength in the first manipulation of a NW and every next manipulation is due to time dependence of static friction (or contact aging). Here we would discuss some possible reasons of contact aging. Silicon is a covalently bonded material that undergoes no plastic deformation in its bulk form and fracture in a brittle manner when the deformation exceeds a few percent. However, recent experiments performed by Ishida et al. with in situ HRTEM had shown extremely high plasticity of silicon nanocontacts at room temperature with a yielding stress $\sigma_{yield} = 2.8$ GPa [41]. Han et al. reported plastic deformation of crystalline Si nanowires at room temperature at the center of the NW [42]. They observed strain-induced structural evolution from crystalline to amorphous in the central part of the stretched NWs. It is also known that crystalline silicon (Si-I) undergoes a phase transformation to a metallic β-Sn (Si-II) phase during loading at a pressure of 8.8 to 16 GPa. Because Si-II is unstable at pressures below 2 GPa, the material undergoes further transformation during pressure release [43]. Haberl et al. demonstrated in nanoindentation experiments a pressure-induced amorphous-to-crystalline phase transformation in amorphous Si at room temperature [44].

Considering that asperities in direct contact with the NW experience vdW forces that attract the entire NW to the surface below it, asperities are subjected to significant compressing stresses (up to 2.5 GPa in the center of asperity, or 3/2 of averaged pressure value [35], *Supplementary data*). At such high pressures, phase transition and plastic deformation of amorphous silicon are possible. Reconfiguration of sharp asperities in contact with the NW can happen due to plastic deformation or slow stress-assisted diffusion of surface atoms from the area of high pressure in the center of asperity to its periphery. As a consequence, elastic deformation gives way to plastic deformation resulting in a relaxation of the elastic force in the compressed asperities. Sharp asperities become flatter, and the real contact area, adhesion forces and static friction increase. This phenomenon indicates the extreme importance of considering plastic deformation when calculating the vdW force in nanoscale contacts even for materials that are hard and brittle in their bulk form.

The process of reconfiguration and flattening of asperities may contribute the contact aging. Contact aging phenomena is not well studied yet. Probably, contact aging involves interdiffusion of atoms of contacting surface [21] or even chemical interactions [45]. Time-dependent static friction resets to minimal value every time the NW is moved to a new position on the substrate. Aging results in significant difference of interfacial shear strength for values for aged contact (the first manipulation of a NW) and newly formed (the second manipulation made within few minutes after the first displacement). After displacement of a NW "traces" frequently can be seen on a substrate in former place of NW (*Supplementary Data*). We noticed this phenomenon for ZnO NWs on SiO_2 surface inside SEM and at ambient conditions after AFM manipulation. Bordag et al. observed "traces" for InAs NW on SiO_2 substrate at ambient AFM manipulation [13]. The fact of "traces" formation can be interpreted as reconfiguration of NW-substrate contact. A detailed investigation of this phenomenon is beyond the scope of this research and a special study should be dedicated to understand contact aging in more detail.

7. Conclusions

We have analyzed the effect of surface roughness on static friction of NWs on flat substrates, and demonstrated approximately an order of magnitude decrease, i.e., from 5.8 to 0.6 nN/nm on average, in the static friction on rough surfaces (RMS roughness is 16.1 nm) compared with smooth surfaces (RMS roughness is 0.7 nm). The elastic bending profile of a NW during the manipulation process was used to find the maximum static friction force. Interfacial shear strength was estimated using real contact area, which was found through a multiple elastic asperity model based on the DMT contact mechanics. Static friction (and interfacial shear strength) decrease significantly (6 times in average) in next manipulation following the first experiment, and this fact was interpreted as manifestation of contact aging.

Acknowledgements

P.K. was supported by ESF Grant no. 2009/0202/1DP/1.1.1.2.0/09/APIA/VIAA/141. B.P. was supported by the Estonian Science Foundation (ETF grant JD162), ESF FANAS program "Nanoparma" and European Union through the European Regional Development Fund (Centre of Excellence "Mesosystems: Theory and Applications", TK114). The work was also partly supported by ETF grants 8420, 9007 and the Estonian Nanotechnology Competence Centre (EU29996).

Appendix A. Supplementary data

Supplementary data to this article can be found online at http://dx.doi.org/10.1016/j.susc.2012.04.029.

References

[1] B. Bhushan, Nanotribology and Nanomechanics, Springer-Verlag, Berlin Heidelberg, 2011.
[2] B. Bhushan, Wear 259 (2005) 1507.
[3] C. Ritter, M. Heyde, B. Stegemann, K. Rademann, Phys. Rev. B 71 (2005) 085405.
[4] B. Bhushan, Handbook of Nanotechnology, Springer-Verlag, Berlin Heidelberg, 2004.
[5] Z. Wang, Mater. Sci. Eng., R 64 (2009) 33.
[6] X. Han, G. Jing, X. Zhang, R. Ma, X. Song, J. Xu, Z. Liao, N. Wang, D. Yu, Nano Res. 2 (2009) 553.
[7] R. He, P. Yang, Nat. Nanotechnol. 1 (2006) 42.
[8] P. Neuzil, C. Wong, J. Reboud, Nano Lett. 10 (2010) 1248.
[9] R. He, X. Feng, M. Roukes, P. Yang, Nano Lett. 8 (2008) 1756.
[10] H. He, C. Hsin, J. Liu, L. Chen, Z. Wang, Adv. Mater. 19 (2007) 781.
[11] P. Kim, C. Lieber, Science 286 (1999) 2148.
[12] K. Ziegler, D. Lyons, J. Holmes, D. Erts, B. Polyakov, H. Olin, K. Svensson, E. Olsson, Appl. Phys. Lett. 84 (2004) 4074.
[13] M. Bordag, A. Ribayrol, G. Conache, L.E. Fröberg, S. Gray, L. Samuelson, L. Montelius, H. Pettersson, Small 3 (2007) 1398.
[14] M. Strus, R. Lahiji, P. Ares, V. Lopez, A. Raman, R. Reifenberger, Nanotechnology 20 (2009) 385709.
[15] L. Dorogin, B. Polyakov, A. Petruhins, S. Vlassov, R. Lohmus, I. Kink, A. Romanov, J. Mater. Res. 27 (2012) 580.
[16] M. Manoharan, M. Haque, J. Phys. D: Appl. Phys. 42 (2009) 095304.
[17] J. Hsu, S. Chang, Appl. Surf. Sci. 256 (2010) 1769.
[18] S. Kim, D. Ratchford, X. Li, ASC Nano 3 (2009) 2989.
[19] S. Vlassov, B. Polyakov, L. Dorogin, A. Lõhmus, A. Romanov, I. Kink, E. Gnecco, R. Lohmus, Solid State Commun. 151 (2011) 688.
[20] G. Conache, S. Gray, A. Ribayrol, L. Froberg, L. Samuelson, H. Pettersson, L. Montelius, Small 5 (2009) 203.
[21] B. Persson, Sliding Friction, second ed. Springer-Verlag, Berlin Heidelberg New York, 2000 G.
[22] N. Tambe, B. Bhushan, Nanotechnology 15 (2004) 1561.
[23] F. Delrio, M. de Boer, J. Knapp, E. Davidreed, P. Clews, M. Dunn, Nat. Mater. 4 (2005) 629.
[24] B. Polyakov, L. Dorogin, S. Vlassov, I. Kink, A. Romanov, R. Lohmus, Micron (2012), http://dx.doi.org/10.1016/j.micron.2012.01.009.
[25] E. Tan, Y. Zhu, T. Yu, L. Dai, C. Sow, V.C. Tan, C. Lim, Appl. Phys. Lett. 90 (2007) 163112.
[26] L. Landau, E. Lifshitz, Theory of Elasticity, Butterworth-Heinemann, Oxford, 1986.
[27] X. Jiang, T. Herricks, Y. Xia, Nano Lett. 2 (2002) 1333.
[28] M. Vila, C. Diaz-Guerra, J. Piqueras, J. Phys. D: Appl. Phys. 43 (2010) 135403.
[29] J.B. Liang, N. Kishi, T. Soga, T. Jimbo, Appl. Surf. Sci. 257 (2010) 62.
[30] K. Sawicka, M. Karadge, P.I. Gouma, Microsc. Microanal. 10 (2004) 360.
[31] B.V. Derjaguin, V.M. Muller, Y.U.P. Toporov, J. Colloid Interface Sci. 53 (1975) 314.

[32] L. Freund, S. Suresh, Thin Film Materials, Cambridge University Press, Cambridge, 2003.
[33] K.A. Reinhardt, W. Kern, Handbook of silicon wafer cleaning technology Attractive Forces at Interfaces, second ed. William Andrew, New York, 2008.
[34] A.A. Ogwu, E. Bouquerel, O. Ademosu, S. Moh, E. Crossan, F. Placido, Acta Mater. 53 (2005) 5151.
[35] J. Israelachvili, Intermolecular and surface forces, Academic Press, London, 1992.
[36] A. Parsegian, Van der Waals Forces, A handbook for biologist, chemists, engineers, and physicists, Cambridge University Press, New York, 2006.
[37] Y. Mo, K. Turner, I. Szlufarska, Nature 457 (2009) 1116.
[38] B. Bhushan, M. Nosonovsky, Acta Mater. 51 (2003) 4331.
[39] J. Hirth, J. Lothe, Theory of dislocations, second ed. J. Wiley and Sons, New York, 1982.
[40] R.W. Carpick, N. Agrait, D.F. Ogletree, M. Salmeron, Langmuir 12 (1996) 3334.
[41] T. Ishida, F. Cleri, K. Kakushima, M. Mita, T. Sato, M. Miyata, N. Itamura, J. Endo, H. Toshiyoshi, N. Sasaki, D. Collard, H. Fujita, Nanotechnology 22 (2011) 355704.
[42] X. Han, K. Zheng, Y. Zhang, X. Zhang, Z. Zhang, Z. Wang, Adv. Mater. 19 (2007) 2112.
[43] B. Haberl, J. Bradby, M. Swain, J. Williams, P. Munroe, Appl. Phys. Lett. 85 (2004) 5559.
[44] R. Gassilloud, C. Ballif, P. Gasser, G. Buerki, J. Michler, Phys. Status Solidi A 202 (2005) 2858.
[45] J. Brndiar, R. Turansky, D. Dietzel, A. Schirmeisen, I. Stich, Nanotechnology 22 (2011) 085704.